Micron 189 (2025) 103747

Contents lists available at ScienceDirect

Micron

journal homepage: www.elsevier.com/locate/micron

A tale of two transfers: characterizing polydimethylsiloxane viscoelastic stamping and heated poly bis-A carbonate transfer of hexagonal boron nitride

Pia Bhatia [a], Trey T. Shin [a,b], Kyril Kavetsky [a,b], Benjamin N. Sailors [a,b], George Siokos [a], Alexandra Sofia Uy-Tioco [a,b], Rachael N. Keneipp [a], Jordan A. Gusdorff [b,c], Lee C. Bassett [c], Marija Drndić [a,*]

[a] Department of Physics and Astronomy, University of Pennsylvania, Philadelphia, PA 19104, USA
[b] Department of Materials Science and Engineering, University of Pennsylvania, Philadelphia, PA 19104, USA
[c] Quantum Engineering Laboratory, Department of Electrical and Systems Engineering, University of Pennsylvania, Philadelphia, PA 19104, USA

ARTICLE INFO

Keywords:
Hexagonal boron nitride (hBN)
Electron energy loss spectroscopy (EELS)
Aberration-corrected scanning transmission electron microscopy (AC-STEM)
Viscoelastic stamping
Dry transfer
Poly bis-A carbonate (PC)
Polydimethylsiloxane (PDMS)
2D materials

ABSTRACT

Two-dimensional (2D) materials have many applications ranging from heterostructure electronics to nanofluidics and quantum technology. In order to effectively utilize 2D materials towards these ends, they must be transferred and integrated into complex device geometries. In this report, we investigate two conventional methods for the transfer of 2D materials: viscoelastic stamping with polydimethylsiloxane (PDMS) and a heated transfer with poly bis-A carbonate (PC). We use both methods to transfer mechanically-exfoliated flakes of hexagonal boron nitride onto silicon nitride (SiN_x) substrates and characterize the resulting transfers using atomic force microscopy (AFM), aberration-corrected scanning transmission electron microscopy (AC-STEM) and electron energy loss spectroscopy (EELS). We find that *both* transfer methods yield flakes with significant and comparable residue (within the limitations of our study on eight samples). Qualitative interpretation of EELS maps demonstrates that this residue is comprised of silicon, carbon and oxygen for both transfer methods. Quantitative analysis of AC-STEM images reveals that the area covered in residue is on average, slightly lower for PDMS transfers (31 % ± 1 %), compared to PC transfers (41 % ± 4 %). This work underscores the importance of improving existing transfer protocols towards applications where cleaner materials are critical, as well as the need for robust methods to clean 2D materials.

1. Introduction

Beginning with the isolation of graphene in 2004 by Geim and Novoselov, interest in two-dimensional (2D) materials research has increased significantly over the past two decades (Novoselov et al., 2005, 2004; Sebastian et al., 2021). Graphene is one of many kinds of van der Waals (vdW) materials, which are a class of crystalline materials whose layers are weakly bound together by vdW interactions (Guo et al., 2021). In order to leverage the unique properties of such materials, researchers typically employ the following workflow: (1) material preparation, (2) transfer, and (3) characterization. To prepare 2D materials, there are two dominant methodologies: mechanical exfoliation and chemical vapor deposition (CVD). Mechanical exfoliation, also referred to as the "Scotch Tape Method," is a process whereby mechanical force is applied to a bulk crystal to obtain atomically thin flakes. This method is used to sequentially and quickly exfoliate layers of vdW material and can be considered a "top-down approach" to fabrication (Gautam and Chelliah, 2021; Mas-Ballesté et al., 2011). In contrast, CVD utilizes gaseous precursors and high temperatures to grow flakes and/or films of vdW materials on various substrates. In this way, CVD can be considered a "bottom-up" approach (Lee et al., 2017; Li et al., 2018; Mandyam et al., 2020; Muñoz and Gómez-Aleixandre, 2013).

Once atomically thin flakes have been acquired, the next challenge is to reliably place the flakes onto target substrates. Transfer methods are typically categorized as either "dry transfers" or "wet transfers" depending on the medium and techniques used (Cheliotis and Zergioti, 2024). Generally, the dry transfer process utilizes a polymer – typically a viscoelastic polymer like polydimethylsiloxane (PDMS) – to

* Corresponding author.
E-mail address: drndic@physics.upenn.edu (M. Drndić).

https://doi.org/10.1016/j.micron.2024.103747
Received 20 June 2024; Received in revised form 10 October 2024; Accepted 12 November 2024
Available online 14 November 2024

"pick-and-place" single flakes on target substrates (Castellanos-Gomez et al., 2014; Toyoda et al., 2019). Meanwhile, the wet transfer method typically utilizes a wet etchant to separate the 2D material from its substrate, resulting in flakes suspended in a polymer layer (often polymethyl methacrylate, or PMMA). This stack can then be placed onto the target substrate where the polymer is subsequently removed (He et al., 2019; Jang et al., 2023). Due to widespread interest in 2D materials, optimization of the transfer process has attracted significant discussion (Bae et al., 2010; Gant et al., 2020; Leong et al., 2019; Yoon et al., 2022; Zhao et al., 2020). Each transfer method has unique advantages and disadvantages, with cleanliness, mechanical damage, and strain being critical factors to consider depending on the desired application.

After transfer, flakes of 2D materials must be appropriately characterized. Many techniques are available to characterize these materials, such as atomic force microscopy (AFM), scanning tunnelling microscopy, Raman spectroscopy, photoluminescence (PL) spectroscopy and imaging, scanning electron microscopy, electronic transport measurements, and transmission electron microscopy (TEM). TEM, and particularly aberration-corrected scanning TEM (AC-STEM) can achieve atomic resolution, thereby providing significant insight into the relationship between atomic structure, defect density, and material properties (Sohn et al., 2024). Moreover, many TEMs are also equipped with detectors that enable in-situ spectroscopy, such as electron energy loss spectroscopy (EELS) or energy dispersive x-ray spectroscopy, yielding critical information about the chemical composition of samples (Marks et al., 2020; Yu and García de Abajo, 2020).

In this paper, we use AC-STEM and EELS to investigate and compare two dry-transfer methods towards the preparation of clean hexagonal boron nitride (hBN) flakes: polydimethylsiloxane (PDMS) viscoelastic stamping and a heated poly bis-A carbonate (PC) transfer. These two methods were chosen as they are widely used in the field (Guo et al., 2021; Jain et al., 2018; Jayasena and Melkote, 2015; Keneipp et al., 2024; Somphonsane, Buapan, and Ramamoorthy, 2024). HBN was selected as a model 2D material due to the significant interest it has garnered in recent years. Also referred to as "white graphene," hBN is a vdW material comprised of alternating boron and nitrogen atoms arranged in a honeycomb lattice. HBN is a wide band-gap semiconductor (~6 eV) that has long been used as an insulating layer in heterostructure electronics (Dean et al., 2010; Knobloch et al., 2021; Molaei et al., 2021). In addition, hBN has captured the attention of the nanofluidics community, owing to its reportedly large intrinsic surface charge, making the material attractive for osmotic power generation applications, nanopore sensing applications, and as a platform to investigate ion transport and fluid dynamics at the nanoscale (Joly et al., 2021; Keneipp et al., 2024; Manikandan et al., 2024; Siria et al., 2013; Weber et al., 2017; Won and Aluru, 2007; Yazda et al., 2021).

In addition to nanofluidics, hBN is also of interest in quantum optics. In 2016, hBN was found to host room-temperature single photon emitters (SPEs) (Tran et al., 2016). As a result, the material has emerged as a promising host for quantum technologies due to its large bandgap, bright single-photon emission, and room-temperature single spins (2017; Exarhos et al., 2019; Jungwirth et al., 2016; Patel et al., 2022, Patel et. al., 2024). The exact chemical nature of SPEs in hBN is an outstanding question, and several mechanisms have been theoretically proposed, including carbon substitutions, boron vacancies, and nitrogen vacancies within hBN's lattice (Tawfik et al., 2017). Several groups have presented evidence that emission in hBN is related to the presence of carbon, often introduced via ion implantation (Auburger and Gali, 2021; Mendelson et al., 2021; Sajid and Thygesen, 2020; Zhong et al., 2024). This raises questions about the interplay, if any, between carbonaceous contamination resulting from the exfoliation and transfer of hBN, which typically involve carbon-rich polymers, and its quantum emission properties (Gusdorff et al., 2024).

In this work, we mechanically exfoliated and transferred eight flakes of hexagonal boron nitride (hBN) using PDMS viscoelastic stamping and heated poly bis-A carbonate (PC) transfer methods. All flakes were transferred over sub-micron holes milled in silicon nitride (SiN_x) membranes. These samples were investigated in detail with AFM, AC-STEM and EELS. Four flakes were prepared using the PDMS viscoelastic stamping method (samples denoted as A, C, D and E), while the other four were prepared using the heated PC method (samples denoted as B, F, G and H). Results from samples A and B are included in the main text, and the results from other samples are included in the Supplementary Information. These exfoliation and transfer methods yielded multilayer flakes of varying thicknesses (~6 nm to 11 nm, as measured by AFM) and relatively large areas (hundreds of square microns). A JEOL NEOARM AC-STEM operating at 80 kV was then used to directly visualize contamination resulting from the sample preparation methods employed. Finally, EELS elemental maps reveal the chemical composition of contamination found on hBN flakes. Our work shows that *both* PDMS viscoelastic stamping and heated PC transfers result in significant contamination on hBN flakes and that this contamination is primarily composed of silicon, carbon, and oxygen species. Within the limitations of our study, which are outlined in the discussion, we conclude to first order, that both transfer methods yield samples of similar quality in terms of cleanliness, as defined by the presence of extraneous silicon, carbon and oxygen on hBN flakes. The percentage of flake area covered in residue was also calculated based on pixel intensity in AC-STEM images for all samples. This analysis shows that PDMS transfers display less residue (31 % ± 1 %), in comparison to PC transfers (41 % ± 4 %).

2. Materials and methods

2.1. Substrate fabrication

For all samples, hBN flakes were transferred over holes milled into 50-nm-thick SiN_x membranes. Holes were patterned into the SiN_x membranes via focused ion beam (FIB) milling in a Tescan S8252X FIB-SEM to suspend the transferred hBN. FIB holes ranged in size from ~ 170 nm to ~ 620 nm in diameter (Chen and Liu, 2019; Peltonen et al., 2016; Thiruraman et al., 2018). The Tescan S8252X ion beam was operated at 30 kV and 10 pA and the scanning electron beam was operated at 5 kV and 30 pA during patterning.

2.2. Viscoelastic transfer

2.2.1. Exfoliation

HBN crystal (HQ Graphene) was mechanically exfoliated onto a 1-inch-wide strip of Nitto SPV 224 tape, with its short edges folded over to create makeshift handles. This tape was placed adhesive side up on a glass microscope slide and referred to as the "mother tape," as shown in Fig. 1(1). A second 1-inch-wide strip of Nitto SPV 224 tape was prepared with makeshift handles. This was referred to as the "daughter tape." Shown in Fig. 1(2), the daughter tape was adhered to the exposed adhesive of the mother tape, and a cotton swab was applied to the back of the daughter tape to ensure contact. After the daughter tape was carefully peeled from the mother tape (Fig. 1(3)), a glass microscope slide carrying two, 4 × 3 arrays of rectangular PDMS blocks (GelPak 3 Gel-Box) on double-sided tape was prepared, as shown in Fig. 1(4). Each individual block roughly measured 4 mm × 2.5 mm. Utilizing rectangular blocks of PDMS instead of square blocks was deliberate, as rectangular blocks allowed for faster and more accurate determination of block orientation, which became important for subsequent steps (see **Section 2.2 .B** and **2.2.C)**. With the PDMS arrays prepared, the daughter tape was then placed into contact with one of the two arrays (see Fig. 1 (5)). Afterwards, the daughter tape was gently removed from the PDMS, leaving the PDMS blocks with hBN on the surface.

2.2.2. Flake selection

The PDMS blocks were surveyed under an optical microscope (Nikon ECLIPSE 80i) to identify thin flakes of hBN. Extremely thin flakes exhibited very little optical contrast with the PDMS, whereas thicker

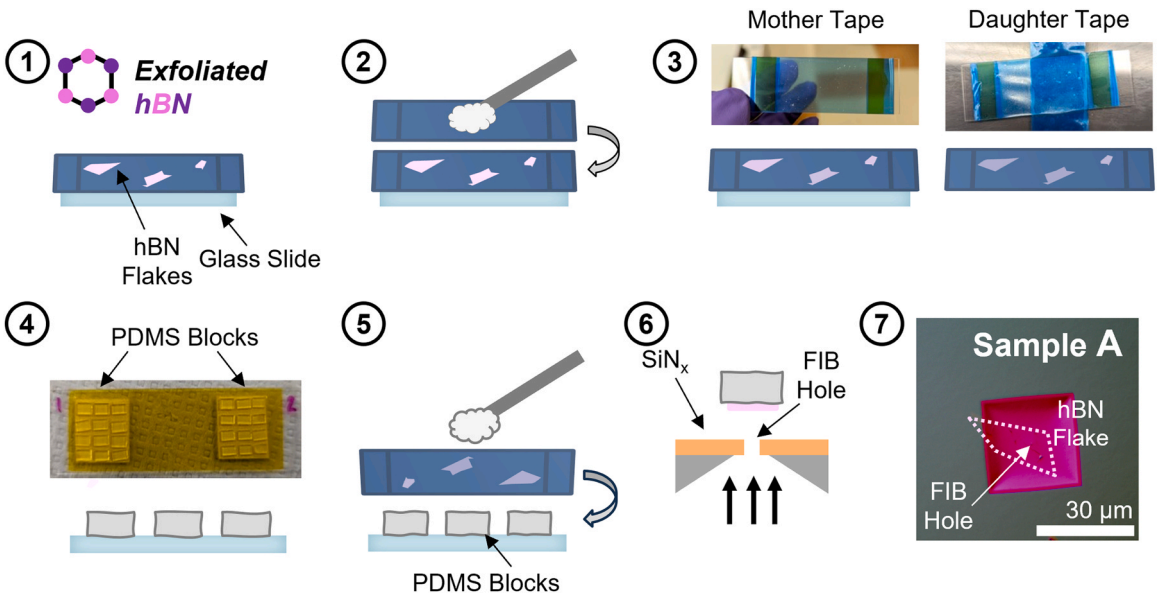

Fig. 1. Schematic of viscoelastic transfer method with PDMS. (1) Mechanically exfoliated hBN flakes (pink) on tape are secured to a glass slide. This tape is referred to as the "mother tape." (2) A cotton swab is used to gently apply pressure to a second piece of tape mutually adhered to the mother tape, yielding a "daughter tape." (3) Mother and daughter tapes, side by side. (4) Prepared PDMS block arrays on a glass microscope slide. (5) HBN flakes are transferred from the daughter tape onto pre-cut PDMS blocks on top of a glass slide. (6) Flakes are then transferred onto target substrates by raising the target until contact is made. Here, the desired substrate is a SiN_x (orange) membrane that has been patterned with a hole. (7) Optical micrograph of Sample A showing transferred hBN flake, outlined with a dashed line.

flakes were easily identifiable. Once an ideal hBN flake was found, its position on the PDMS block was recorded so that the flake could be easily avoided when handling the PDMS block during the transfer process. In general, due to the surface area of a PDMS block being similar in magnitude to that of a target substrate, a single PDMS block usually yielded only one hBN transfer. However, if two hBN flakes of equal desirability were sufficiently separated (i.e. two flakes located at opposite ends of a PDMS block), then two hBN transfers from a single PDMS block could be achieved.

2.2.3. Transfer

The transfer of hBN onto a target substrate was carried out under a different optical microscope, using a micromanipulator and motorized XYZ stage to move the hBN-carrying PDMS block and substrate, respectively. Prior to a transfer, substrates were piranha cleaned together at 200 °C for 30 min and subsequently submerged in deionized water. For a single transfer, a substrate was taken out of the deionized water, thoroughly dried with N_2, and adhered to the motorized stage using double-sided carbon tape. The other substrates remained in the deionized water until they were used in subsequent transfers. Substrates were left in the deionized water for up to two hours with no noticeable impact on the ease or quality of the transfer. The substrate was brought into focus in the microscope, and the FIB hole on the SiN_x window was centered. With the substrate ready, an hBN-carrying PDMS block was carefully removed from the glass microscope slide with tweezers, taking care not to disturb the desired flake, and attached to the "transfer arm." The transfer arm refers to a 0.25-inch × 1-inch × 11.75-inch acrylic bar with a glass microscope slide secured with Scotch tape to one of the 1-inch × 11.75-inch faces, leaving a 1-inch × 1-inch area of the microscope slide protruding beyond the length of the bar. A 1-inch × 1-inch cut of transparent double-sided tape was then placed on the exposed area of the microscope slide, and the hBN-carrying PDMS placed atop the tape. The transfer arm was flipped upside-down such that the exposed hBN faced downward and was secured to the micromanipulator with a large binder clip. Under the microscope, the PDMS block was brought into focus and the desired hBN flake was located and centered. Next, the substrate was slowly raised towards the PDMS block (see Fig. 1(6)) until contact was made to transfer the flake onto the target substrate. The hBN-containing substrate was then brought back to the optical microscope to verify a successful transfer, with an example of such shown in Fig. 1(7). For further information, see Keneipp et al., (2024).

2.3. Heated PC transfer

2.3.1. Exfoliation

HBN crystal was mechanically exfoliated into few-layered flakes by repeated folding in Nitto SPV 224 tape. Silicon wafers with a 285 nm-thick SiO_2 surface layer were cleaved into ~ 1-cm × 1-cm pieces and cleaned in piranha solution at 200 °C for 20 min, followed by 5 min of oxygen plasma cleaning (PSDP Pro, Novascan Technologies, Inc.) This cleaning step removes adsorbates from the oxide surface, improving exfoliation performance and mitigating contamination (Huang et al., 2015). Furthermore, this oxide thickness was used because it has been shown to provide high optical contrast for thin 2D materials (Wang et al., 2012). Tapes containing the flakes were immediately brought into contact with the clean Si/SiO_2 wafer pieces and pressed down to remove air bubbles at the tape-substrate interface. The Si/SiO_2/tape pieces were then annealed at 100 °C for 2 min on a hot plate, cooled to room temperature, and the tape kept pressed down across the entire Si/SiO_2 surface for one minute to remove any trapped gases at the flake-substrate interface (Huang et al., 2015). The tape was subsequently removed from the Si/SiO_2 pieces by gently pulling at a 15 ° to 30 ° angle. This process yielded exfoliated flakes of hBN on the Si/SiO_2 pieces, which are hereby referred to as the "exfoliation substrates." Desirable hBN flakes were identified by surveying the exfoliation substrate under an optical microscope.

2.3.2. Transfer slide preparation

Transfer slides were assembled by affixing small (~ 2 mm × 2 mm × 2 mm) PDMS blocks onto clean glass microscope slides. These PDMS blocks were each patterned with a ~ 50 μm square region by soft lithography. This was done to ensure accurate placement of flakes onto target substrates. We found this step to be critical to the success of the transfer, since thin hBN flakes are virtually invisible when

adhered to the transparent transfer slide. A PC film was prepared by spincoating 8 wt% PC : 92 wt% chloroform solution at 4000 rpm for 60 s onto a piranha cleaned Si/SiO_2 wafer piece. A piece of hole-punched office tape was used to remove the PC film from the Si/SiO_2 spincoating substrate and affix it to the transfer slide such that the patterned face of the PDMS block was covered with the suspended PC film, as shown in Fig. 2(1).

2.3.3. Flake selection & transfer

The exfoliation substrate and target substrate were loaded onto the sample stage, the transfer slide was loaded onto the transfer arm, and the stage temperature was set to 40 °C (Fig. 2(2)). The desired hBN flake was brought into view through the PDMS block and the transfer slide was lowered until contact with the exfoliation substrate was established. The stage temperature was then increased to 60 °C, and passively cooled to 30 °C (Fig. 2(3) and 2(4)). After cooling, the transfer slide was removed from the exfoliation substrate, resulting in the adhesion of hBN flake to

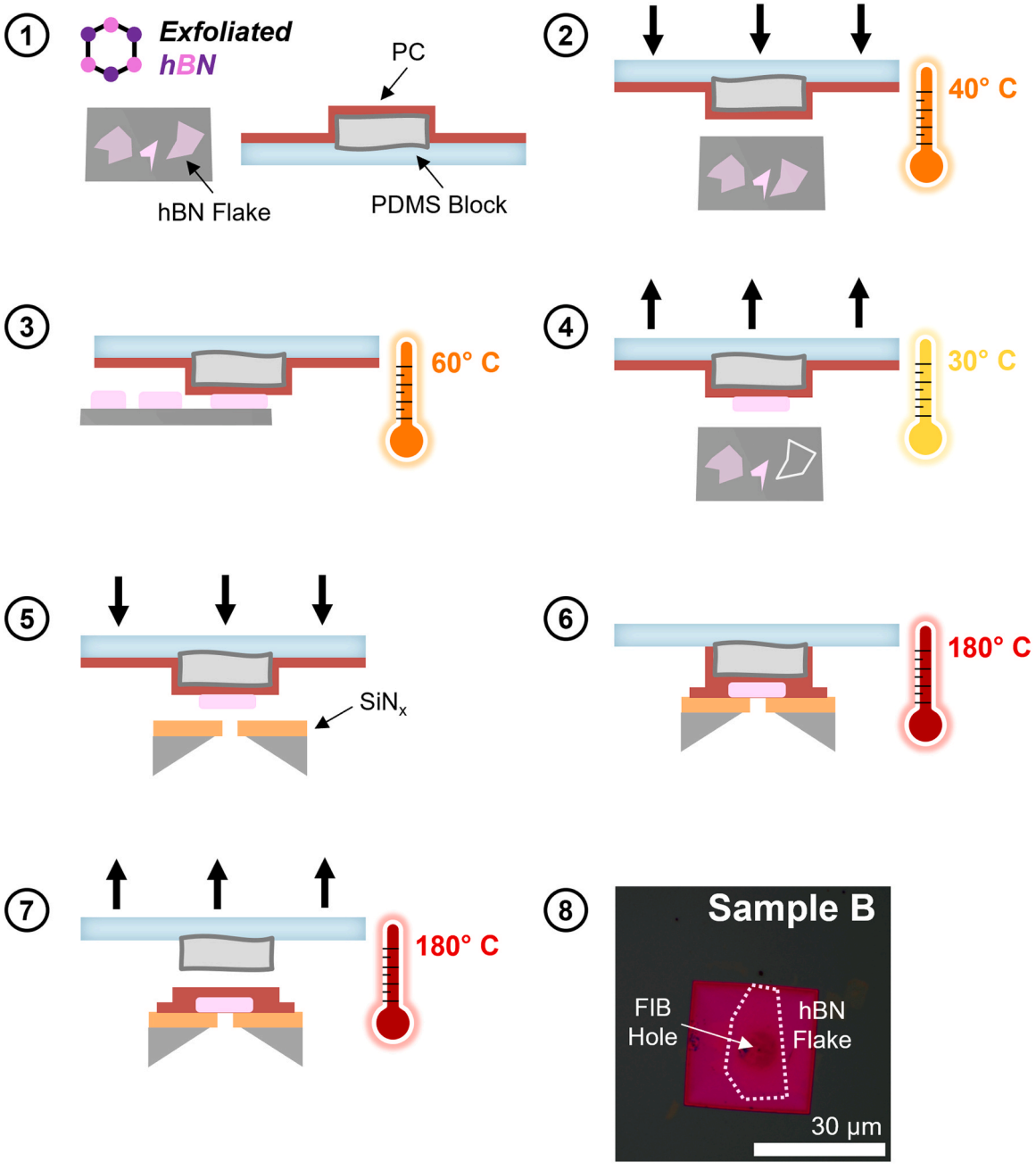

Fig. 2. Schematic of heated transfer method with PC. (1) Mechanically exfoliated hBN flakes (pink) are prepared on an Si/SiO_2 substrate; this is the "exfoliation substrate." A PDMS block on a glass slide is coated with PC (red); this is the "transfer slide." (2) With the heated stage set to 40 °C, the transfer slide is lowered onto the exfoliation substrate. (3) Once the transfer slide has made contact with the desired hBN flake, the stage temperature is raised to 60 °C. (4) Upon reaching 60 °C the stage is allowed to cool to 30 °C and the transfer slide is lifted from the exfoliation substrate with the desired flake adhered to the PC film. (5) The flake is aligned with the target substrate and slowly lowered until contact is made. Here, the target substrate is a SiN_x membrane (orange) that has been patterned with a hole. (6) Once contact is made, the stage temperature is raised to 180 °C to melt the PC. (7) The PDMS block is raised from the interface, leaving the desired flake and a film of PC on the target substrate. (8) Optical micrograph of Sample B with the transferred flake outlined with a dashed line. This micrograph was taken after rinsing away the layer of PC in heated (60 °C) chloroform for 5 min.

the PC-coated PDMS blocks. Finally, the hBN flake was aligned above the target substrate Fig. 2(5) with the assistance of the lithographically patterned PDMS. The stage temperature was then increased to 180 °C until the PC film completely melted, disestablishing contact between the hBN flakes and the PDMS (Fig. 2(6)). The transfer slide was raised from the target substrate and the stage was allowed to cool to room temperature. The target substrate was then soaked in heated (60 °C) chloroform to remove residual PC from the transferred hBN.

2.4. Atomic force microscopy

The thickness of all flakes was measured using either a Bruker Icon AFM or a Bruker Multimode 8 AFM. All AFM data was processed in Gwyddion. For all AFM scans, background removal was performed and a line profile was drawn over the edge of the flake to determine the approximate flake thickness (see Fig. S1).

2.5. AC-STEM imaging & EELS

AC-STEM imaging and EELS were performed on a JEOL NEOARM STEM operating at 80 kV with a ~ 37 pA probe current* and a 4 cm camera length. AC-STEM imaging utilized a Gatan annular dark field (ADF) detector. All images were captured with a 1024 × 1024 px^2 resolution and 32 μs/px dwell time, and subsequently processed in ImageJ. EELS spectrum images were collected with a Gatan Quantum GIF equipped with an Ultrascan camera. All spectrum images were captured with a 0.25 eV/ch dispersion, 166.8 × 166.8 nm^2 size, 110 × 110 px^2 resolution, and a 0.005 s per pixel dwell time, with the exception of Sample H. The EEL spectrum image for Sample H was captured with a 0.25 eV/ch dispersion, 126.3 × 126.3 nm^2 size, 95 × 95 px^2 resolution, and a 0.001 s per pixel dwell time. All spectrum images were processed in Gatan's GMS software as follows: (1) when applicable, spurious x-rays were filtered from spectrum images (Bosman and Keast, 2008); (2) a first-order-log-polynomial background subtraction was applied to each spectrum image, with a 19 eV-wide background fit window beginning at 75 eV; (4) when applicable, EELS maps were cropped to only include regions of suspended hBN; (5) Elemental maps of boron, carbon, nitrogen, oxygen and silicon were produced by integrating the signal intensity of the summed spectra from each spectrum image. Each map is normalized with respect to its maximum intensity.

* *The reported AC-STEM probe current was obtained from JEOL and measured when the JEOL NEOARM was installed at the University of Pennsylvania.*

2.6. Sample storage

After the transfer of hBN, and in between AC-STEM, EELS, and AFM characterizations, all samples were stored in GelPaks under vacuum. Samples were exposed to air during transfer, AC-STEM specimen exchange, and AFM measurements. Note that when samples were in GelPaks, they were stored with the hBN flake facing upwards at all times (i.e., no contact with the PDMS film). Our substrate geometry is such that there is a ~ 300 μm gap between the bottom of the substrate and the bottom surface of the hBN flake when samples are stored in this orientation.

3. Results and discussion

We characterized hBN samples prepared either by PDMS stamping or heated PC transfer using AC-STEM, EELS, and AFM (see Supporting Information, Table S1). Fig. 3 shows Sample A, a 6-nm-thick flake prepared by PDMS stamping, and its associated AC-STEM and EELS data. The sample is covered in a non-uniform layer of residue (Fig. 3(c)) and elemental maps taken from the same region indicate that the residue-rich regions are primarily composed of silicon (Fig. 3(d)). Qualitatively, it appears that the oxygen and carbon signals are also spatially correlated with the residue shown in Fig. 3. However, the overall strength of the carbon and oxygen signals is much weaker in comparison to that of silicon for Sample A. Similar results are observed for Samples C, D, and E (Figs. S2-S4), which were also prepared via PDMS stamping.

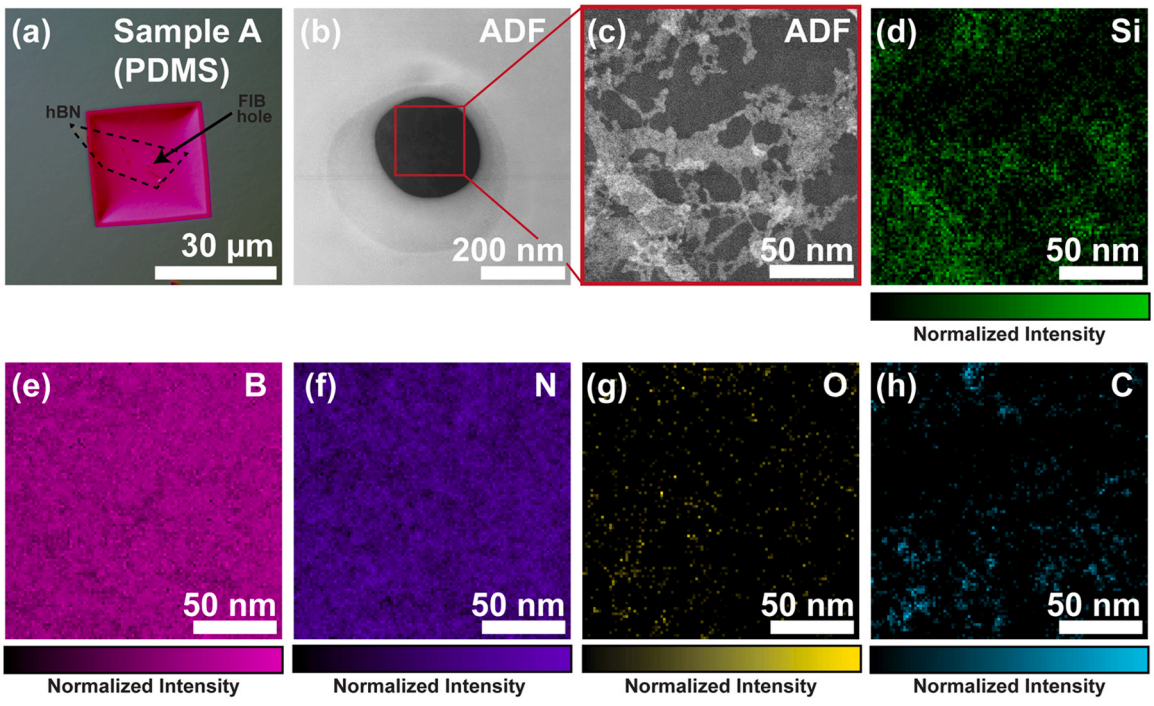

Fig. 3. EELS map of Sample A prepared via PDMS stamping. (a) Optical micrograph showing suspended hBN flake on an SiN_x membrane. (b) ADF image showing an hBN flake suspended over a FIB hole. The region boxed in red corresponds to the next panel. (c) ADF image corresponding to the EELS elemental maps shown in the remaining panels. (d-h) EELS elemental maps indicating the presence of silicon, boron, nitrogen, oxygen and carbon, respectively. Black corresponds to the absence of an element, and color indicates its presence.

Like Sample A, the silicon, carbon, and oxygen elemental maps for Samples C, D and E appear to be qualitatively correlated with the contaminated regions shown in their respective ADF images (Fig. S2(c), Fig. S3(c), and Fig. S4(c)). For Samples C through E, the silicon maps consistently display the strongest correlation with the residue, followed by the carbon map, with the oxygen map having the weakest correlation (Fig. S2(d-h), Fig. S3(d-h), and Fig. S4(d-h), respectively). The presence of a particularly strong silicon signal, and more moderate carbon and oxygen signals in the residue-rich regions of Samples A, C, D and E is consistent with the composition of the PDMS blocks used to prepare these samples. PDMS is comprised of a repeating silicon and oxygen backbone, with two methyl groups branching off of each silicon atom. Furthermore, it is not surprising that a thin layer of PDMS may adhere to flakes during the transfer process given that the polymer's adhesive properties are in part what makes the material an effective viscoelastic stamp (Jain, et al., 2018; Vlassov et al., 2018).

Similarly, we characterized four samples transferred using the heated PC method. Fig. 4 shows Sample B, a 7-nm-thick flake prepared in this way. We observed that Sample B is covered in residue (Fig. 4(c)) and that like the PDMS-transferred samples, this residue is strongly correlated with the presence of silicon (Fig. 4(d)). This result was somewhat surprising, given that in the PC-transfer method, the suspended region of hBN did not have direct contact with any silicon-containing materials (i.e., PDMS). Instead, the flake was shielded by a thin layer of PC, which does *not* contain silicon (Kim et al., 2008). This suggests that the residue observed is influenced by additional factors, which may be worth further investigation. For example, silicon could arise from the substrates themselves which contain SiN_x and/or the substrate milling process; storage methods (such as PDMS-lined Gel-Paks); or environmental contaminants, given that all transfers were performed in air using shared equipment, as opposed to inside a dedicated glovebox or cleanroom environment. Another potential source of silicon might be the diffusion of un-crosslinked PDMS oligomers through the PC film to the surface of hBN flakes (Jain et al., 2018; Lee et al., 2003; Regehr et al., 2009).

The oxygen and carbon maps of Sample B (Fig. 4(g)-(h)) exhibit qualitatively weaker spatial correlation with the residue shown in the ADF image (Fig. 4(c)), which is similar to the PDMS stamped samples. Here, the weaker carbon and oxygen signals may be attributed to the final heated chloroform soak, which was intended to dissolve the melted PC. Samples F, G and H replicate what was observed in Sample B (Figs. S5, S6, and S7, respectively). Namely, Samples F, G and H are also covered in a silicon-rich residue, with weaker contributions from carbon and oxygen.

Fig. 5 summarizes the normalized EEL spectra across all eight samples, and shows no observable difference between PDMS and PC-transferred samples. For all samples, the boron K-edge and nitrogen K-edge signals are the strongest, followed by slight peaks corresponding to the silicon $L_{2,3}$ edge. In the plot of all normalized spectra, it is difficult to discern peaks corresponding to the carbon K-edge and oxygen K-edge for any samples. This indicates that relatively few carbon and oxygen counts were captured by the EELS detectors for all samples, in comparison to those collected for silicon, boron, and nitrogen. For all samples, the silicon signal is consistently the strongest (greatest intensity), followed by the carbon signal, and the oxygen signal is the weakest, demonstrated by the EELS maps and Fig. 5.

It is also interesting to compare the annular dark field (ADF) images obtained across samples. These images show that contamination does not uniformly cover the suspended regions of hBN for either the PC or PDMS samples. Moreover, ADF images indicate that where contamination is present on hBN flakes, the contamination itself is not of uniform thickness. (This is justified because in ADF images, the intensity is proportional to thickness, with thicker regions appearing more bright/white, and thinner regions appearing more dark/black.) This qualitative observation can be expanded upon, by quantifying the relative amount of residue on all samples. A simple image processing routine (see Fig. S8 in the Supplementary Information) was performed on all ADF images (Figs. 3(c), 4(c), S2(c)-S7(c)) to determine the average residue coverage on PDMS transferred samples (31 % ± 1 %) and PC transferred samples (41 % ± 4 %). This analysis reveals that there a statistically significant

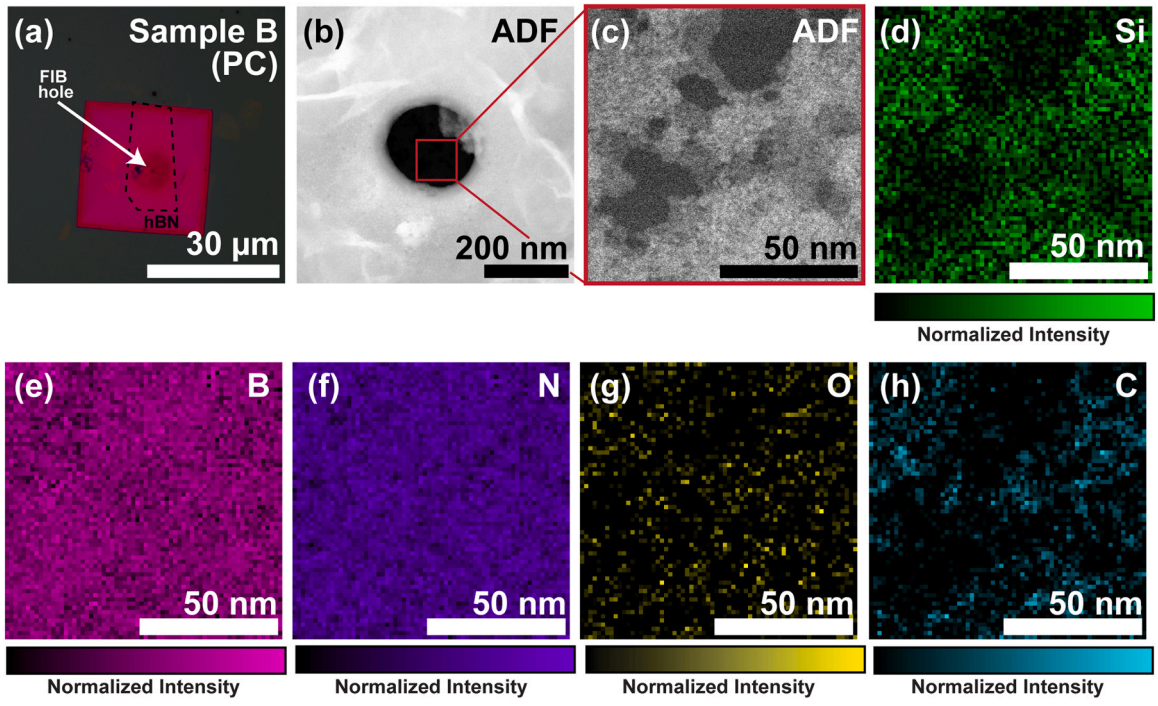

Fig. 4. EELS map of Sample B prepared via heated PC transfer. (a) Optical micrograph showing suspended hBN flake on an SiN_x membrane. (b) ADF image showing an hBN flake suspended over a FIB hole. The region boxed in red corresponds to the next panel. (c) ADF image corresponding to the EELS elemental maps shown in the remaining panels. (d-h) EELS elemental maps indicating the presence of silicon, boron, nitrogen, oxygen and carbon, respectively. Black corresponds to the absence of an element, and color indicates its presence.

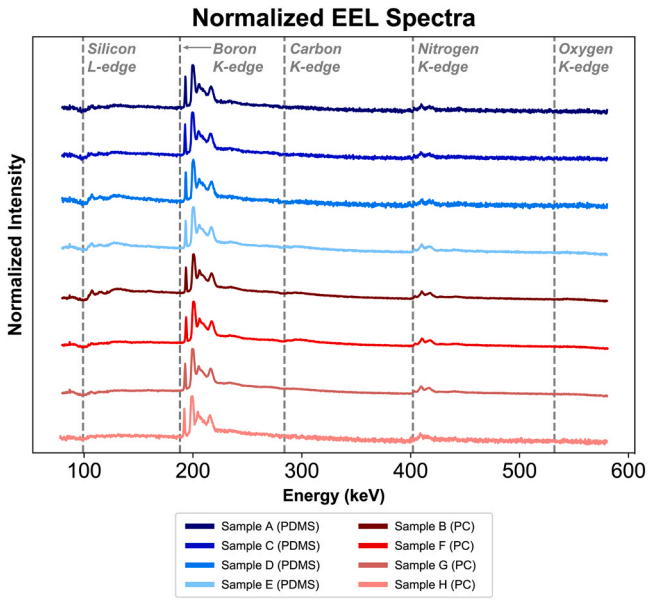

Fig. 5. Normalized EEL spectra for all samples. Plotted spectra corresponding to the EELS maps shown in Figs. 3, 4, and the SI. Each spectrum is produced by summing the single spectrum collected at each pixel, over all pixels in the spectrum image obtained for each sample. Samples prepared via PDMS stamping are shown in shades of blue. Samples prepared via PC transfer and are shown in shades of red. All spectra were normalized by dividing by the highest signal intensity prior to plotting. The location of the silicon $L_{2,3}$ (99 keV), boron K (188 keV), carbon K (284 keV), nitrogen K (402 keV), and oxygen K (532 keV) edge onsets are marked with grey dashed lines.

difference in the relative amounts of residue for the two transfer methods. Furthermore, the coverage varied slightly more within PC samples than PDMS samples because the standard deviation is greater for PC samples (4 %) than PDMS samples (1 %).

4. Conclusions

In conclusion, we report and evaluate two transfer methods for preparing few-layer, suspended hBN flakes over holes in SiN_x membranes: viscoelastic stamping with PDMS and a heated PC transfer technique. AC-STEM and EELS mapping revealed the presence of significant residue regardless of transfer method. Qualitative interpretation of EELS maps indicates that in both cases, the residue is composed primarily of silicon, with weaker contributions from carbon and oxygen. In the case of PDMS viscoelastic stamping, this observation is consistent with the chemical structure of PDMS itself. However, for heated PC transfers, the presence of silicon is somewhat counterintuitive and may indicate that residue arises from alternative sources. This indicates that further study is necessary to determine with certainty the source of the silicon-rich residue on PC-transferred samples. In contrast, quantitative analysis of AC-STEM images did reveal observable differences between the two methods. Samples transferred via PDMS viscoelastic stamping, on average, displayed relatively less residue in comparison to samples prepared with the heated PC transfer method.

Multiple limitations exist within our study. First, our study includes only eight samples, which necessarily limits the statistical significance of our results. Second, our study exclusively focused on two dry transfer methods: PDMS stamping and heated PC transfer. It would certainly be of interest to explore contamination resulting from wet transfer methods and additional dry transfer procedures with AFM, AC-STEM, and EELS. Third, electron irradiation may modify the structure and quantity of contamination (Egerton, 2019; Egerton et al., 2004). Care was taken to acquire all AC-STEM data and EELS maps with the minimum exposure necessary, but this effect cannot be altogether ignored. Furthermore, in the case of hBN, outstanding questions regarding the interplay between contamination and the material's desirable optoelectronic properties may be better addressed by studies utilizing techniques, such as PL and/or Raman spectroscopies in addition to AFM, AC-STEM and EELS (Gusdorff et al., 2024). Finally, this study did not investigate potential cleaning treatments for transferred flakes, which may remedy contamination. Despite its limitations, this work employing a detailed elemental analysis contributes to the growing body of literature on the effects of contamination on 2D materials, and sheds light on the pervasive issue of contamination in 2D materials sample preparation, with a focus on hBN.

CRediT authorship contribution statement

Pia Bhatia: Writing – review & editing, Writing – original draft, Visualization, Investigation, Data curation, Conceptualization. **Trey T. Shin:** Writing – review & editing, Writing – original draft, Visualization, Investigation, Data curation. **Kyril Kavetsky:** Writing – review & editing, Writing – original draft, Visualization, Investigation, Data curation. **Benjamin Sailors:** Writing – review & editing, Writing – original draft, Visualization, Investigation. **George Siokos:** Investigation, Writing – review & editing. **Alexandra Sofia Uy-Tioco:** Data curation, Writing – review & editing. **Rachael N. Keneipp:** Writing – review & editing, Writing – original draft, Visualization, Investigation, Data curation, Conceptualization. **Jordan A. Gusdorff:** Writing – review & editing. **Lee C. Bassett:** Writing – review & editing. **Marija Drndić:** Writing – review & editing, Supervision, Resources, Project administration, Conceptualization..

Declaration of Competing Interest

The authors declare the following financial interests/personal relationships which may be considered as potential competing interests: Marija Drndic reports a relationship with Goeppert that includes: consulting or advisory. All other authors declare that they have no known competing financial interests or personal relationships that could have appeared to influence the work reported in this paper.

Acknowledgements

This work was primarily supported by DOE grant DE-SC0023224 on advanced in-situ TEM analysis and ex-situ studies of 2D hBN. M.D. lab also acknowledges support from NIH grant R01HG01241 for the development of hBN/graphene nanopores. J.A.G. and L.C.B acknowledge support from NSF award DMR-1922278, and NSF award DMR-2019444. J.A.G. acknowledges support from NSF Graduate Research Fellowship (DGE-1845298. AC-STEM imaging, EELS, and substrate fabrication were carried out at the Singh Center for Nanotechnology at the University of Pennsylvania, which is supported by the NSF National Nanotechnology Coordinated Infrastructure Program under grant NNCI-2025608. The authors also gratefully acknowledge use of facilities and instrumentation supported by NSF through the University of Pennsylvania Materials Research Science and Engineering Center (MRSEC) (DMR-1720530). The authors wish to thank Dr. Douglas Yates for his assistance with AC-STEM imaging and EELS, as well as Dr. Jamie Ford for his assistance with FIB milling.

Appendix A. Supporting information

Supplementary data associated with this article can be found in the online version at doi:10.1016/j.micron.2024.103747.

Data Availability

Data will be made available on request.

References

Auburger, P., Gali, A., 2021. Towards ab initio identification of paramagnetic substitutional, carbon defects in hexagonal boron nitride acting as quantum bits. Phys. Rev. B 104, 075410. https://doi.org/10.1103/PhysRevB.104.075410.

Bae, S., Kim, H., Lee, Y., Xu, X., Park, J.-S., Zheng, Y., Balakrishnan, J., Lei, T., Ri Kim, H., Song, Y.I., Kim, Y.-J., Kim, K.S., Özyilmaz, B., Ahn, J.-H., Hong, B.H., Iijima, S., 2010. Roll-to-roll production of 30-inch graphene films for transparent electrodes. Nat. Nanotechnol. 5, 574–578. https://doi.org/10.1038/nnano.2010.132.

Bosman, M., Keast, V.J., 2008. Optimizing EELS acquisition. Ultramicroscopy 108, 837–846. https://doi.org/10.1016/j.ultramic.2008.02.003.

Castellanos-Gomez, A., Buscema, M., Molenaar, R., Singh, V., Janssen, L., Zant, H.S.J. van der, Steele, G.A., 2014. Deterministic transfer of two-dimensional materials by all-dry. viscoelastic stamping. 2D Mater. 1, 011002. https://doi.org/10.1088/2053-1583/1/1/011002.

Chejanovsky, N., Mukherjee, A., Geng, J., Chen, Y.C., Kim, Y., Denisenko, A., Finkler, A., Taniguchi, T., Watanabe, K., Dasari, D.B.R., Auburger, P., Gali, A., Smet, J.H., Wrachtrup, J., 2021. Single-spin resonance in a van der Waals embedded paramagnetic defect. Nat. Mater. 20, 1079–1084. https://doi.org/10.1038/s41563-021-00979-4.

Cheliotis, I., Zergioti, I., 2024. A review on transfer methods of two-dimensional materials. 2D Mater. 11, 022004. https://doi.org/10.1088/2053-1583/ad2f43.

Chen, Q., Liu, Z., 2019. Fabrication and applications of solid-state nanopores. Sensors 19, 1886. https://doi.org/10.3390/s19081886.

Dean, C.R., Young, A.F., Meric, I., Lee, C., Wang, L., Sorgenfrei, S., Watanabe, K., Taniguchi, T., Kim, P., Shepard, K.L., Hone, J., 2010. Boron nitride substrates for high-quality graphene electronics. Nat. Nanotechnol. 5, 722–726. https://doi.org/10.1038/nnano.2010.172.

Egerton, R.F., 2019. Radiation damage to organic and inorganic specimens in the TEM. Micron 119, 72–87. https://doi.org/10.1016/j.micron.2019.01.005.

Egerton, R.F., Li, P., Malac, M., 2004. Radiation damage in the TEM and SEM. Micron, Int. Wuhan. Symp. Adv. Electron Microsc. 35, 399–409. https://doi.org/10.1016/j.micron.2004.02.003.

Exarhos, A.L., Hopper, D.A., Grote, R.R., Alkauskas, A., Bassett, L.C., 2017. Optical signatures of quantum emitters in suspended hexagonal boron nitride. ACS Nano 11, 3328–3336. https://doi.org/10.1021/acsnano.7b00665.

Exarhos, A.L., Hopper, D.A., Patel, R.N., Doherty, M.W., Bassett, L.C., 2019. Magentic-field-dependent quantum emission in hexagonal boron nitride at room temperature. Nat. Commun. 10, 222. https://doi.org/10.1038/s41467-018-08185-8.

Gant, P., Carrascoso, F., Zhao, Q., Ryu, Y.K., Seitz, M., Prins, F., Frisenda, R., Castellanos-Gomez, A., 2020. A system for the deterministic transfer of 2D materials under inert. environmental conditions. 2D Mater. 7, 025034. https://doi.org/10.1088/2053-1583/ab72d6.

Gautam, C., Chelliah, S., 2021. Methods of hexagonal boron nitride exfoliation and its functionalization: covalent and non-covalent approaches. RSC Adv. 11, 31284–31327. https://doi.org/10.1039/D1RA05727H.

Guo, H.-W., Hu, Z., Liu, Z.-B., Tian, J.-G., 2021. Stacking of 2D materials. Adv. Funct. Mater. 31, 2007810. https://doi.org/10.1002/adfm.202007810.

Gusdorff, J.A., Bhatia, P., Shin, T.T., Sailors, B.N., Uy-Tioco, A.S., Keneipp, R.N., Drndić, M., Bassett, L.C., 2024. Correlated Structural and Optical Characterization of Hexagonal Boron Nitride. doi:10.48550/arXiv.2411.14408.

He, T., Wang, Z., Zhong, F., Fang, H., Wang, P., Hu, W., 2019. Etching techniques in 2D. materials. Adv. Mater. Technol. 4, 1900064. https://doi.org/10.1002/admt.201900064.

Huang, Y., Sutter, E., Shi, N.N., Zheng, J., Yang, T., Englund, D., Gao, H.-J., Sutter, P., 2015. Reliable exfoliation of large-area high-quality flakes of graphene and other two- dimensional materials. ACS Nano 9, 10612–10620. https://doi.org/10.1021/acsnano.5b04258.

Jain, A., Bharadwaj, P., Heeg, S., Parzefall, M., Taniguchi, T., Watanabe, K., Novotny, L., 2018. Minimizing residues and strain in 2D materials transferred from PDMS. Nanotechnology 29, 265203. https://doi.org/10.1088/1361-6528/aabd90.

Jang, D.J., Haidari, M.M., Kim, J.H., Ko, J.-Y., Yi, Y., Choi, J.S., 2023. A modified wet. transfer method for eliminating interfacial impurities in graphene. Nanomaterials 13, 1494. https://doi.org/10.3390/nano13091494.

Jayasena, B., Melkote, S.N., 2015. An Investigation of PDMS Stamp Assisted Mechanical Exfoliation of Large Area Graphene Procedia Manuf., 43rd North Am. Manuf. Res. Conf., NAMRC 43, 8-12 June 2015, UNC Charlotte, North Carol., U. S.184085310.1016/j.promfg.2015.09.073.

Joly, L., Meißner, R.H., Iannuzzi, M., Tocci, G., 2021. Osmotic transport at the aqueous. graphene and hBN interfaces: scaling laws from a unified, first-principles description. ACS Nano 15, 15249–15258. https://doi.org/10.1021/acsnano.1c05931.

Jungwirth, N.R., Calderon, B., Ji, Y., Spencer, M.G., Flatté, M.E., Fuchs, G.D., 2016. Temperature dependence of wavelength selectable zero-phonon emission from single defects in hexagonal boron nitride. Nano Lett. 16, 6052–6057. https://doi.org/10.1021/acs.nanolett.6b01987.

Keneipp, R.N., Gusdorff, J.A., Bhatia, P., Shin, T.T., Bassett, L.C., Drndić, M., 2024. Nanoscale sculpting of hexagonal boron nitride with an electron beam. J. Phys. Chem. C 128, 8741–8749. https://doi.org/10.1021/acs.jpcc.4c02038.

Kim, J., Gracz, H.S., Roberts, G.W., Kiserow, D.J., 2008. Spectroscopic analysis of poly (bisphenol A carbonate) using high resolution 13C and 1H NMR. Polymer 49, 394–404. https://doi.org/10.1016/j.polymer.2007.11.046.

Knobloch, T., Illarionov, Y.Y., Ducry, F., Schleich, C., Wachter, S., Watanabe, K., Taniguchi, T., Mueller, T., Waltl, M., Lanza, M., Vexler, M.I., Luisier, M., Grasser, T., 2021. The performance limits of hexagonal boron nitride as an insulator for scaled CMOS devices based on two-dimensional materials. Nat. Electron 4, 98–108. https://doi.org/10.1038/s41928-020-00529-x.

Lee, H.C., Liu, W.-W., Chai, S.-P., Mohamed, A.R., Aziz, A., Khe, C.-S., Hidayah, N.M.S., Hashim, U., 2017. Review of the synthesis, transfer, characterization and growth. mechanisms of single and multilayer graphene. RSC Adv. 7, 15644–15693. https://doi.org/10.1039/C7RA00392G.

Lee, J.N., Park, C., Whitesides, G.M., 2003. Solvent compatibility of Poly (dimethylsiloxane)- based microfluidic devices. Anal. Chem. 75, 6544–6554. https://doi.org/10.1021/ac0346712.

Leong, W.S., Wang, H., Yeo, J., Martin-Martinez, F.J., Zubair, A., Shen, P.-C., Mao, Y., Palacios, T., Buehler, M.J., Hong, J.-Y., Kong, J., 2019. Paraffin-enabled graphene transfer. Nat. Commun. 10, 867. https://doi.org/10.1038/s41467-019-08813-x.

Li, H., Li, Y., Aljarb, A., Shi, Y., Li, L.-J., 2018. Epitaxial growth of two-dimensional layered transition-metal dichalcogenides: growth mechanism, controllability, and scalability. Chem. Rev. 118, 6134–6150. https://doi.org/10.1021/acs.chemrev.7b00212.

Mandyam, S.V., Kim, H.M., Drndić, M., 2020. Large area few-layer TMD film growths and their applications. J. Phys. Mater. 3, 024008. https://doi.org/10.1088/2515-7639/ab82b3.

Manikandan, D., Karishma, S., Kumar, M., Nayak, P.K., 2024. Salinity gradient induced blue energy generation using two-dimensional membranes. NPJ 2D Mater. Appl. 8, 1–19. https://doi.org/10.1038/s41699-024-00486-5.

Marks, S., Pinard, P., Burgess, S., Bithell, J., Beanland, R., 2020. Measuring the thickness of 2D materials using EDS. Microsc. Micro 26, 1212–1214. https://doi.org/10.1017/S1431927620017353.

Mas-Balleste, R., Navarro, C., Gómez-Herrero, J., Zamora, F., 2011. 2D materials: to graphene and beyond. Nanoscale 3, 20–30. https://doi.org/10.1039/c0nr00323a.

Mendelson, N., Chugh, D., Reimers, J.R., Cheng, T.S., Gottscholl, A., Long, H., Mellor, C. J., Zettl, A., Dyakonov, V., Beton, P.H., Novikov, S.V., Jagadish, C., Tan, H.H., Ford, M.J., Toth, M., Bradac, C., Aharonovich, I., 2021. Identifying carbon as the source of visible single-photon emission from hexagonal boron nitride. Nat. Mater. 20, 321–328. https://doi.org/10.1038/s41563-020-00850-y.

Molaei, M.J., Younas, M., Rezakazemi, M., 2021. A comprehensive review on recent. advances in Two-Dimensional (2D) hexagonal boron nitride. ACS Appl. Electron. Mater. 3, 5165–5187. https://doi.org/10.1021/acsaelm.1c00720.

Muñoz, R., Gómez-Aleixandre, C., 2013. Review of CVD synthesis of graphene. Chem. Vap. Depos. 19, 297–322. https://doi.org/10.1002/cvde.201300051.

Novoselov, K.S., Geim, A.K., Morozov, S.V., Jiang, D., Zhang, Y., Dubonos, S.V., Grigorieva, I.V., Firsov, A.A., 2004. Electric field effect in atomically thin carbon films. Science 306, 666–669. https://doi.org/10.1126/science.1102896.

Novoselov, K.S., Jiang, D., Schedin, F., Booth, T.J., Khotkevich, V.V., Morozov, S.V., Geim, A.K., 2005. Two-dimensional atomic crystals. Proc. Natl. Acad. Sci. 102, 10451–10453. https://doi.org/10.1073/pnas.0502848102.

Patel, R.N., Fishman, R.E.K., Huang, T., Gusdorff, J.A., Fehr, D.A., Hopper, D., Breitweiser, A., Porat, S.A., Flatté, B., Bassett, L. C, M.E., 2024. Room temperature dynamics of an optically addressable single spin in hexagonal boron nitride. Nano Lett. 24, 7623–7628. https://doi.org/10.1021/acs.nanolett.4c01333.

Patel, R.N., Hopper, D.A., Gusdorff, J.A., Turiansky, M.E., Huang, T.-Y., Fishman, R.E.K., Porat, B., Van de Walle, C.G., Bassett, L.C., 2022. Probing the optical dynamics of quantum emitters in hexagonal boron nitride. PRX Quantum 3, 030331. https://doi.org/10.1103/PRXQuantum.3.030331.

Peltonen, A., Nguyen, H.Q., Muhonen, J.T., Pekola, J.P., 2016. Milling a silicon nitride. membrane by focused ion beam. J. Vac. Sci. Technol. B 34, 062201. https://doi.org/10.1116/1.4963895.

Regehr, K.J., Domenech, M., Koepsel, J.T., Carver, K.C., Ellison-Zelski, S.J., Murphy, W. L., Schuler, L.A., Alarid, E.T., Beebe, D.J., 2009. Biological implications of polydimethylsiloxane-based microfluidic cell culture. Lab Chip 9, 2132–2139. https://doi.org/10.1039/B903043C.

Sajid, A., Thygesen, K.S., 2020. VNCB defect as source of single photon emission from hexagonal boron nitride. 2D Mater. 7, 031007. https://doi.org/10.1088/2053-1583/ab8f61.

Sebastian, A., Pendurthi, R., Choudhury, T.H., Redwing, J.M., Das, S., 2021. Benchmarking monolayer MoS2 and WS2 field-effect transistors. Nat. Commun. 12, 693. https://doi.org/10.1038/s41467-020-20732-w.

Siria, A., Poncharal, P., Biance, A.-L., Fulcrand, R., Blase, X., Purcell, S.T., Bocquet, L., 2013. Giant osmotic energy conversion measured in a single transmembrane boron nitride nanotube. Nature 494, 455–458. https://doi.org/10.1038/nature11876.

Sohn, W., Kim, M., Jang, H.W., 2024. Atomic-scale insights into the 2D materials from aberration-corrected scanning transmission electron microscopy: progress and future. Small Sci. 4, 2300073. https://doi.org/10.1002/smsc.202300073.

Somphonsane, R., Buapan, K., Ramamoorthy, H., 2024. Advances in 2D material transfer systems for van der Waals heterostructure assembly. Appl. Sci. 14, 6341. https://doi.org/10.3390/app14146341.

Tawfik, S.A., Ali, S., Fronzi, M., Kianinia, M., Tran, T.T., Stampfl, C., Aharonovich, I., Toth, M., Ford, M.J., 2017. First-principles investigation of quantum emission from hBN defects. Nanoscale 9, 13575–13582. https://doi.org/10.1039/C7NR04270A.

Thiruraman, J.P., Fujisawa, K., Danda, G., Das, P.M., Zhang, T., Bolotsky, A., Perea-López, N., Nicolaï, A., Senet, P., Terrones, M., Drndić, M., 2018. Angstrom-size defect creation and ionic transport through pores in single-layer MoS2. Nano Lett. 18, 1651–1659. https://doi.org/10.1021/acs.nanolett.7b04526.

Toyoda, S., Uwanno, T., Taniguchi, T., Watanabe, K., Nagashio, K., 2019. Pinpoint pick-up and bubble-free assembly of 2D materials using PDMS/PMMA polymers with lens shapes. Appl. Phys. Express 12, 055008. https://doi.org/10.7567/1882-0786/ab176b.

Tran, T.T., Elbadawi, C., Totonjian, D., Lobo, C.J., Grosso, G., Moon, H., Englund, D.R., Ford, M.J., Aharonovich, I., Toth, M., 2016. Robust multicolor single photon

emission from point defects in hexagonal boron nitride. ACS Nano 10, 7331–7338. https://doi.org/10.1021/acsnano.6b03602.

Vlassov, S., Oras, S., Antsov, M., Sosnin, I., Polyakov, B., Shutka, A., Krauchanka, M.Yu, Dorogin, L.M., 2018. Adhesion and mechanical properties of PDMS-based materials probed with AFM: a review. Rev. Adv. Mater. Sci. 56, 62–78. https://doi.org/10.1515/rams-2018-0038.

Wang, Y.Y., Gao, R.X., Ni, Z.H., He, H., Guo, S.P., Yang, H.P., Cong, C.X., Yu, T., 2012. Thickness identification of two-dimensional materials by optical imaging. Nanotechnology 23, 495713. https://doi.org/10.1088/0957-4484/23/49/495713.

Weber, M., Koonkaew, B., Balme, S., Utke, I., Picaud, F., Iatsunskyi, I., Coy, E., Miele, P., Bechelany, M., 2017. Boron nitride nanoporous membranes with high surface charge by atomic layer deposition. ACS Appl. Mater. Interfaces 9, 16669–16678. https://doi.org/10.1021/acsami.7b02883.

Won, C.Y., Aluru, N.R., 2007. Water permeation through a subnanometer boron nitride nanotube. https://doi.org/10.1021/ja0687318 J. Am. Chem. Soc. 129, 2748–2749. https://doi.org/10.1021/accountsmr.2c00114.

Yazda, K., Bleau, K., Zhang, Y., Capaldi, X., St-Denis, T., Grutter, P., Reisner, W.W., 2021. High osmotic power generation via nanopore arrays in hybrid hexagonal boron Nitride/Silicon nitride membranes. Nano Lett. 21, 4152–4159. https://doi.org/10.1021/acs.nanolett.0c04704.

Yoon, M.-A., Kim, C., Kim, J.-H., Lee, H.-J., Kim, K.-S., 2022. Surface properties of CVD-grown graphene transferred by wet and dry transfer processes. Sensors 22, 3944. https://doi.org/10.3390/s22103944.

Yu, R., García de Abajo, F.J., 2020. Chemical identification through two-dimensional electron energy-loss spectroscopy. Sci. Adv. 6, eabb4713. https://doi.org/10.1126/sciadv.abb4713.

Zhao, Q., Wang, T., Ryu, Y.K., Frisenda, R., Castellanos-Gomez, A., 2020. An inexpensive system for the deterministic transfer of 2D materials. J. Phys. Mater. 3, 016001. https://doi.org/10.1088/2515-7639/ab6a72.

Zhong, D., Gao, S., Saccone, M., Greer, J.R., Bernardi, M., Nadj-Perge, S., Faraon, A., 2024. Carbon-related quantum emitter in hexagonal boron nitride with homogeneous energy and 3-fold polarization. Nano Lett. 24, 1106–1113. https://doi.org/10.1021/acs.nanolett.3c03628.